Electrical Engineering (2024) 106:1021–1031
https://doi.org/10.1007/s00202-023-02032-w

ORIGINAL PAPER

A dual frequency resonant inverter for different material vessel induction hob

Bhavin Salvi[1] · **S. Porpandiselvi**[1] · **N. Vishwanathan**[1]

Received: 7 March 2023 / Accepted: 6 September 2023 / Published online: 29 September 2023

Abstract
Induction heating (IH) is the most preferred technology for domestic and industrial heating applications owing to its advantages over conventional heating methods. Heating requirements for ferromagnetic (FM) and non-ferromagnetic (N-FM) materials are different. There is an increase in research for heating these different material vessels. In this research work, a three switch dual frequency resonant inverter (3 S-DFRI) with dual frequency control is proposed. It has been used for simultaneous and independent heating of steel and aluminum loads. The inverter operation is verified by rigorous simulation and experimentation on the developed 2 kW prototype. It can also be extended for multiple loads by additional inverter legs each with three switches. Each additional leg provides two independent load operation. Compatibility with different material IH loads, reduced number of switching devices, no use of electro-mechanical switches, compact size and high efficiency are the key advantages of the proposed inverter.

Keywords Induction heating · Resonant power conversion · Induction cooker · Domestic appliances

1 Introduction

Conventional heating methods lead to more wastage of energy and deteriorate the environment [1]. On the contrary, induction heating technique offers a clean, safe and efficient solution for heating applications [2, 3]. In induction heating, a high frequency ac voltage is given to the load which induces high frequency ac currents in the heating object and produces heat due to power dissipation caused by the vessel resistance [4]. In past, several inverter topologies have been proposed for heating ferro-magnetic based materials [5, 6]. These can be divided into mainly single switch [7], half-bridge (HB) [8] and full-bridge (FB) [9] based resonant inverters. These resonant inverter solutions are typically controlled by asymmetric duty cycle [10], asymmetric voltage cancelation [11], pulse density modulation [12] and frequency based control techniques [13–15].

Traditional approach used for heating FM materials is not suitable for heating non-ferro magnetic (N-FM) type materials due to different material characteristics [16]. FM materials are powered with typically 20–30 kHz range frequency as it offers high resistance in that frequency range. But N-FM materials offer very low resistance for lower range of frequencies and its resistance increases with the increase in switching frequency [17]. In order to achieve targeted IH, frequency selectable IH is used in [18]. Variable turn pitch coil is used for inductively heating utensils in [19]. All metal IH solution with load detection control is proposed using two coils with different number of turns in [20]. But this is a heavy and bulky solution. In [21], different material vessels are heated by using fundamental and third harmonic components. The current flowing through N-FM material is very high to meet the power requirements which is not desirable. Dual frequency approach is used in [22] to meet different heating requirements of all metal heating. This approach affects ZVS which impacts the efficiency of the system. FB and HB inverters with load adaptive modulation technique is proposed in [23].

Bhavin Salvi proposed the research concept and performed simulation and experimentation under the supervision of S. Porpandiselvi and N. Vishwanathan. All the authors contributed to the editing and proofreading of this paper.

✉ Bhavin Salvi
sbhavin@student.nitw.ac.in

S. Porpandiselvi
selvi@nitw.ac.in

N. Vishwanathan
nvn@nitw.ac.in

[1] Department of Electrical Engineering, National Institute of Technology Warangal, Warangal, Telangana 506004, India

As per material type, modes to double and triple the frequencies are used. It also uses electro-mechanical switch for capacitor switching. By using sandwiched coil and capacitor switching all utensil heating solution is proposed in [17]. A solution by cascading full bridge circuits is proposed in [24]. But the component count is high. A dual resonant, series and series–parallel circuits for heating vessels of different materials is used in [25]. It also uses an electro-mechanical switch. In the available inverter topologies for all metal IH applications, high component count, bulky solutions, use of electro-mechanical switches are the common limitations.

In order to overcome above mentioned common limitations, a half-bridge with three switches is proposed. This inverter provides two HB inverter operation with three switches. It generates two frequency components in the output to meet heating requirements of FM and N-FM materials. The key advantages offered by the proposed inverter with dual frequency control are as follows:

(i) Low number of device count for multi-load different material induction cooking applications.
(ii) Simultaneous as well as independent control for multi-load IH applications.
(iii) Soft-switching operation which increases the efficiency.
(iv) Extension with additional three switches for two different IH loads.
(v) No use of electro-mechanical switches.

Further this paper is organised from Sects. 2 to 7. Section 2 describes the inverter topology with control. Operating modes of the inverter are discussed in Sect. 3. Mathematical expressions for output power control is derived in Sect. 4. Experimental results are discussed in Sect. 5. Major conclusions are presented in Sect. 7.

2 Inverter topology and control technique

Circuit diagram of the proposed resonant inverter is as shown in Fig. 1. It comprises of a dc source (V), split capacitors (C_4 and C_5), three switching devices (S_1, S_2 and S_3) and two different material IC loads (steel and aluminum) with their respective series resonant capacitors. Steel and aluminum loads are modeled as '$R_1 - L_1$' and '$R_2 - L_2$', respectively. Capacitors C_{rs} and C_{ra} resonate steel and aluminum load at their respective resonant frequencies.

The proposed control logic is presented in Fig. 2. It generates gate pulses for the three switching devices as shown in Fig. 3. This control meets the different frequency heating requirement of the ferro and non-ferromagnetic material IC loads with three switches. The switching frequency of switch S_1 decides the operating frequency for steel load. The switching frequency of S_2 and S_3 when S_1 is ON decides the

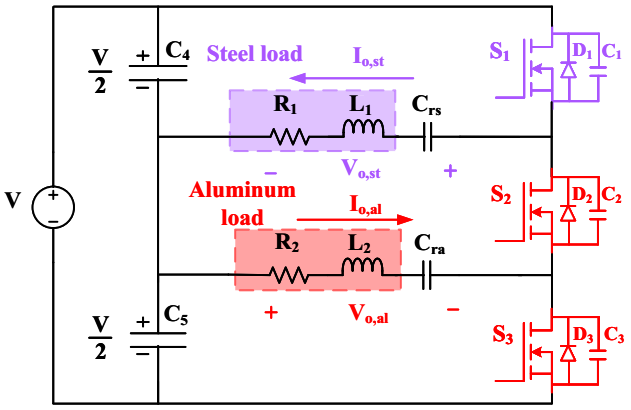

Fig. 1 Proposed three switch dual frequency resonant inverter

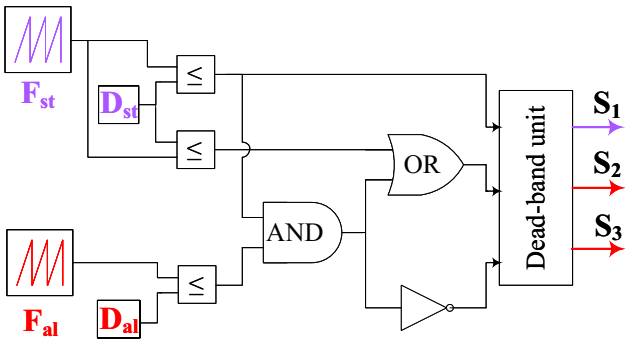

Fig. 2 Dual frequency control logic

operating frequency for aluminum load. The control parameters for the two IC loads can be given as follows.

$$D_{st} = \frac{T_{st,on}}{T_{st}} \qquad f_{st} = \frac{1}{T_{st}} \tag{1}$$

$$D_{al} = \frac{T_{al,on}}{T_{al}} \qquad f_{al} = \frac{1}{T_{al}} \tag{2}$$

where, D_{st}, f_{st} are duty cycle and operating frequency for the steel load and D_{al}, f_{al} are duty cycle and operating frequency for the aluminum load respectively. $T_{st,on}$ and T_{st} are the ON time and total time period of the switch S_1. $T_{al,on}$ and T_{al} are the turn-on and total time period of the switch S_2 when S_1 is ON. S_3 operates in complementary to S_2 when S_1 is ON. Also, both S_2 and S_3 are ON continuously when S_1 is OFF as shown in Fig. 3.

3 Operating modes

The complete operation of the 3 S-DFRI is depicted in Fig. 4 and is divided into following modes.

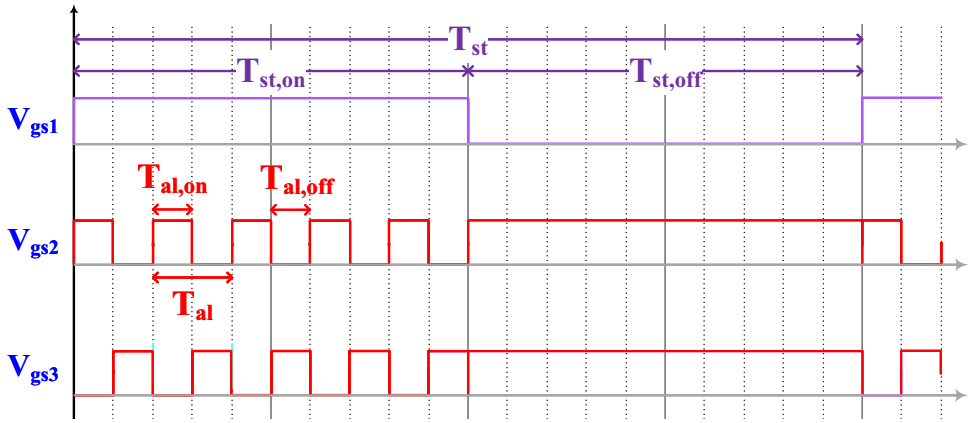

Fig. 3 Gate-pulses for the 3 S-DFRI

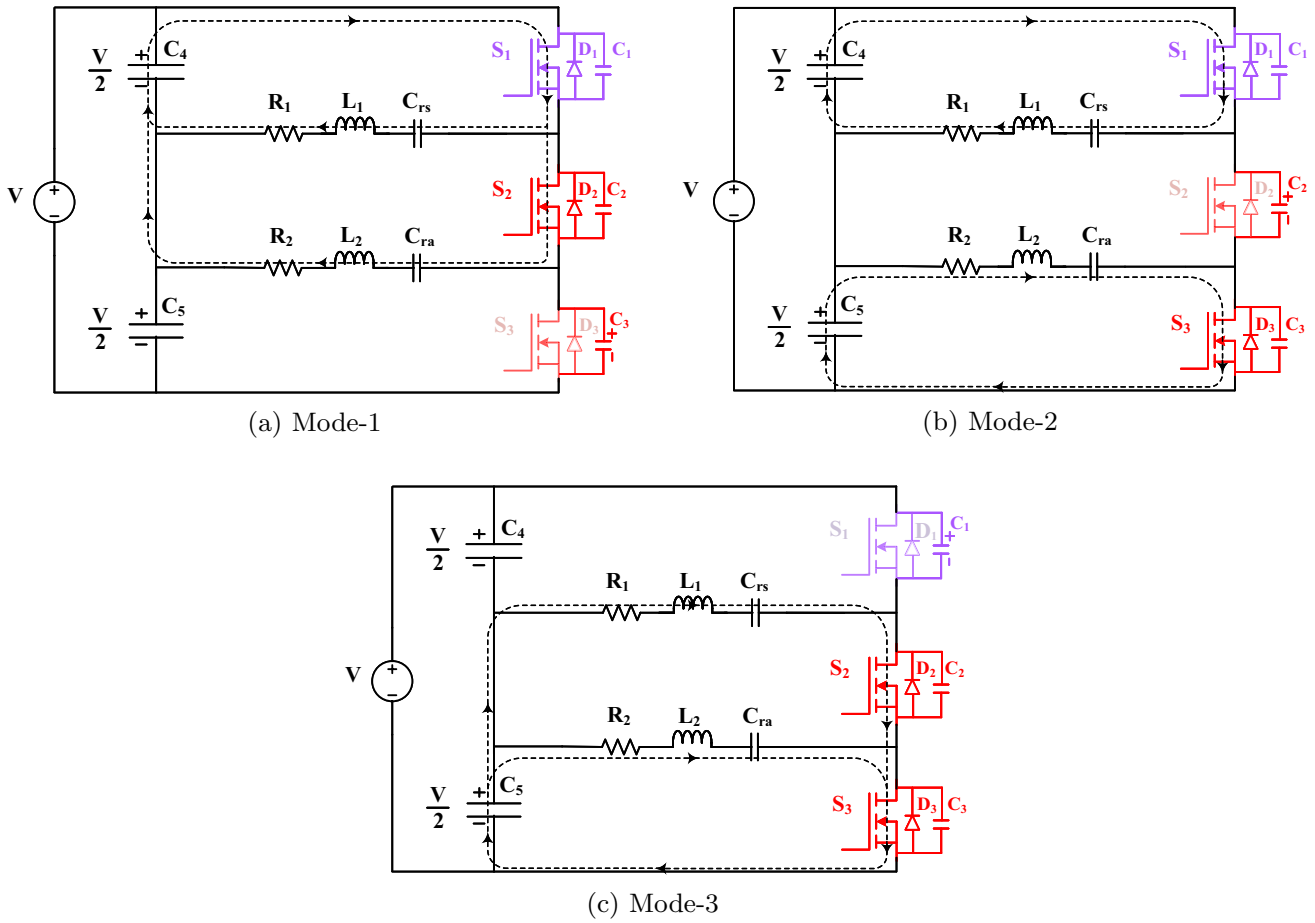

(a) Mode-1

(b) Mode-2

(c) Mode-3

Fig. 4 Operating modes for 3 S-DFRI

3.1 Mode-1

In this mode, S_1 and S_2 are ON and S_3 is OFF as shown in Fig. 4a. Both the loads are powered by C_4. Negative steel load current flows through body diode of S_1 during the transition from mode-3 to mode-1. S_1 is turning ON which was in OFF state during mode-3. The voltage across S_1 is clamped. Hence, ZVS turn-ON of S_1 is obtained. The direction of the currents through both the IH loads is as depicted in Fig. 4a.

3.2 Mode-2

In this mode, S_2 turns-off and S_3 is turning ON. As load current is of lagging nature, negative current will flow though body diode of S_3 in the transition from mode-1 to mode-2.

This ensures zero voltage turn-on of S_3. The load current directions are shown in Fig. 4b.

3.3 Mode-3

During this mode, S_2 is turning ON and S_1 is turning OFF. Steel load current shown in mode-2 will pass through the body diode of S_2 during the transition from mode-2 to mode-3 ensuring ZVS for turn-on of S_2. The state during this mode is depicted in Fig. 4c.

4 Output power control

The resonant frequency for the IH load is given by

$$f_r = \frac{1}{2\pi\sqrt{LC}} \tag{3}$$

where L is equivalent inductor of the IH load and C is resonant capacitor for the loads. Using above equation 3, respective resonant frequencies for steel (f_{rs}) and aluminum (f_{ra}) loads can be obtained for their respective parameters mentioned in Table 1. The switching frequencies are selected a bit higher than their respective resonant frequencies to ensure lagging of load current. It helps in ZVS operation. For steel load, fourier series expression for output voltage $V_{o,st}$ can be expressed as

$$v_{o,st}(t) = \frac{V(2D_{\text{st}} - 1)}{2} + \sum_{n=1}^{\infty} \frac{2V}{n\pi} \sin(n\pi D_{\text{st}}) \cos(n\omega t - n\pi D_{\text{st}}) \tag{4}$$

Using fundamental component, the rms voltage across steel load can be written as

$$V_{\text{o,st,rms}} = \frac{\sqrt{2}V}{\pi} \sin(\pi D_{\text{st}}) \tag{5}$$

$$I_{\text{o,st,rms}} = \frac{\sqrt{2}V \sin(\pi D_{\text{st}})}{\pi} \frac{\cos\psi}{R_1} \tag{6}$$

where,

$$\cos\psi = \frac{1}{\sqrt{1 + Q_{L,st}^2 \left(\frac{\omega}{\omega_o} - \frac{\omega_o}{\omega}\right)^2}} \tag{7}$$

where $Q_{L,st}$ = quality factor for‘ the steel load, ω_o = resonant frequency. Now, the output power equation for steel load can be given by

$$P_{\text{st}} = I_{\text{o,st,rms}}^2 \times R_1 \tag{8}$$

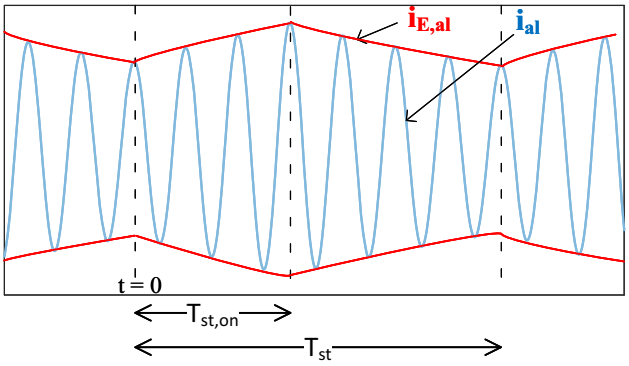

Fig. 5 Aluminum load current and its envelope

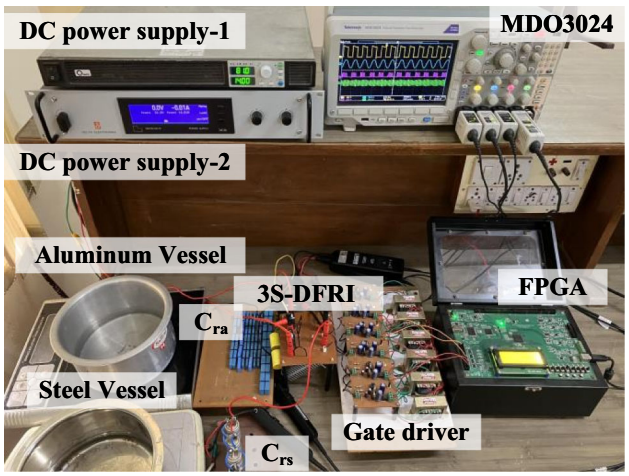

Fig. 6 Hardware setup

$$= \frac{2V^2 \sin^2(\pi D_{\text{st}})}{\pi^2 R_1} \times \frac{1}{1 + Q_{\text{L,st}}^2 \left(\frac{\omega}{\omega_o} - \frac{\omega_o}{\omega}\right)^2} \tag{9}$$

It can be observed from above equations that P_{st} depends on D_{st}. By varying frequency f_{st}, the operating point on resonance curve changes so impedance of the circuit also changes. Hence, steel load current can also be varied by varying f_{st}.

s

For aluminum load, it is getting powered only when switch S_1 is ON i.e., $T_{\text{st,on}}$. As the switch S_1 is turning on and off, the current through the aluminum load, i_{al} is oscillatory as shown in Fig. 5. The envelope of this load current ($i_{\text{E,al}}$) follows first-order response with time constant $\tau = \frac{2L}{R}$. By using the detailed procedure mentioned in [12], the average power in aluminum load can be given by

$$P_{\text{al}} = \frac{2}{\pi} V \cos\alpha \frac{1}{T_{\text{st}}} \int_0^{T_{\text{st,on}}} i_{\text{e,al}}(t)\mathrm{d}t$$

Table 1 Parameters for proposed inverter circuit

Component	Value
DC supply voltages, $2 \times \frac{V}{2}$	$2 \times 82.5 = 165$ V
Steel load equivalent resistance, R_1	2.8 Ω
Steel load equivalent inductance, L_1	66 μH
Resonant capacitor for steel load, C_{rs}	0.52 μF
Aluminum load equivalent resistance, R_2	2 Ω
Aluminum load equivalent inductance, L_2	54 μH
Resonant capacitor for aluminum load, C_{ra}	11 nF
Steel load control frequency, f_{st}	29–44 kHz
Aluminum load control frequency, f_{al}	215–228 kHz
MOSFETs used	IRFP4127PbF
r_{ds} of MOSFETs	17 mΩ

$$= P_{\mathrm{al,m}} \frac{T_{\mathrm{st,on}}}{T_{\mathrm{st}}} + \frac{\tau}{T_{\mathrm{st}}} \left(\frac{1 - e^{\frac{-T_{\mathrm{st,on}}}{\tau}}}{1 - e^{\frac{-T_{\mathrm{st}}}{\tau}}} \right) \left(e^{\frac{-T_{\mathrm{st,on}}}{\tau}} - e^{\frac{-T_{\mathrm{st}}}{\tau}} \right) \tag{10}$$

where $P_{\mathrm{al,m}} = (2/\pi) V I_{\mathrm{al,m}} \cos\alpha$ is the maximum output power for aluminum for when $T_{\mathrm{st,on}} = T_{\mathrm{st}}$. And α is the angle between output voltage and load current. The maximum current can be derived using fourier analysis and is given by

$$I_{\mathrm{al,m}} = \frac{2V}{\pi Z} \sin(\pi D_{\mathrm{al}}) \tag{11}$$

Where, 'Z' is the impedance of aluminum load. Now, for $T_{\mathrm{st}} << \tau$, no oscillations in the output power will occur and the relation can be given by

$$\lim_{\tau \to \infty} P_{\mathrm{al}} = P_{al,m} \left(\frac{T_{\mathrm{st,on}}}{T_{\mathrm{st}}} \right)^2 \tag{12}$$

And for $T_{\mathrm{st}} >> \tau$, the load current will become discontinuous and its equation can be given by

$$\lim_{\tau \to 0} P_{\mathrm{al}} = P_{al,m} \frac{T_{\mathrm{st,on}}}{T_{\mathrm{st}}} \tag{13}$$

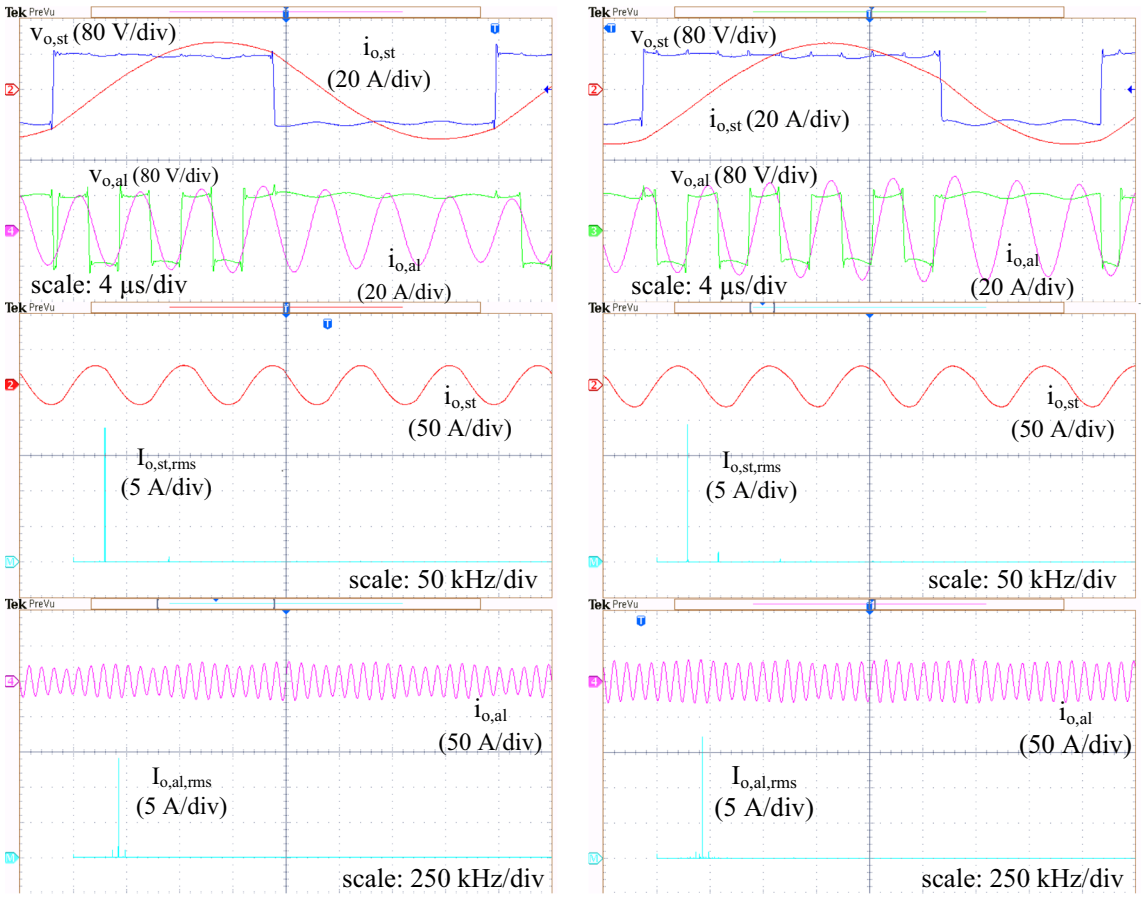

(a) $D_{st} = D_{al} = 50\%$ (b) $D_{st} = 65\%$, $D_{al} = 50\%$

Fig. 7 Experimentation waveforms for full load power operation. From top to bottom: output voltage-current waveforms and load current FFTs for steel and aluminum loads

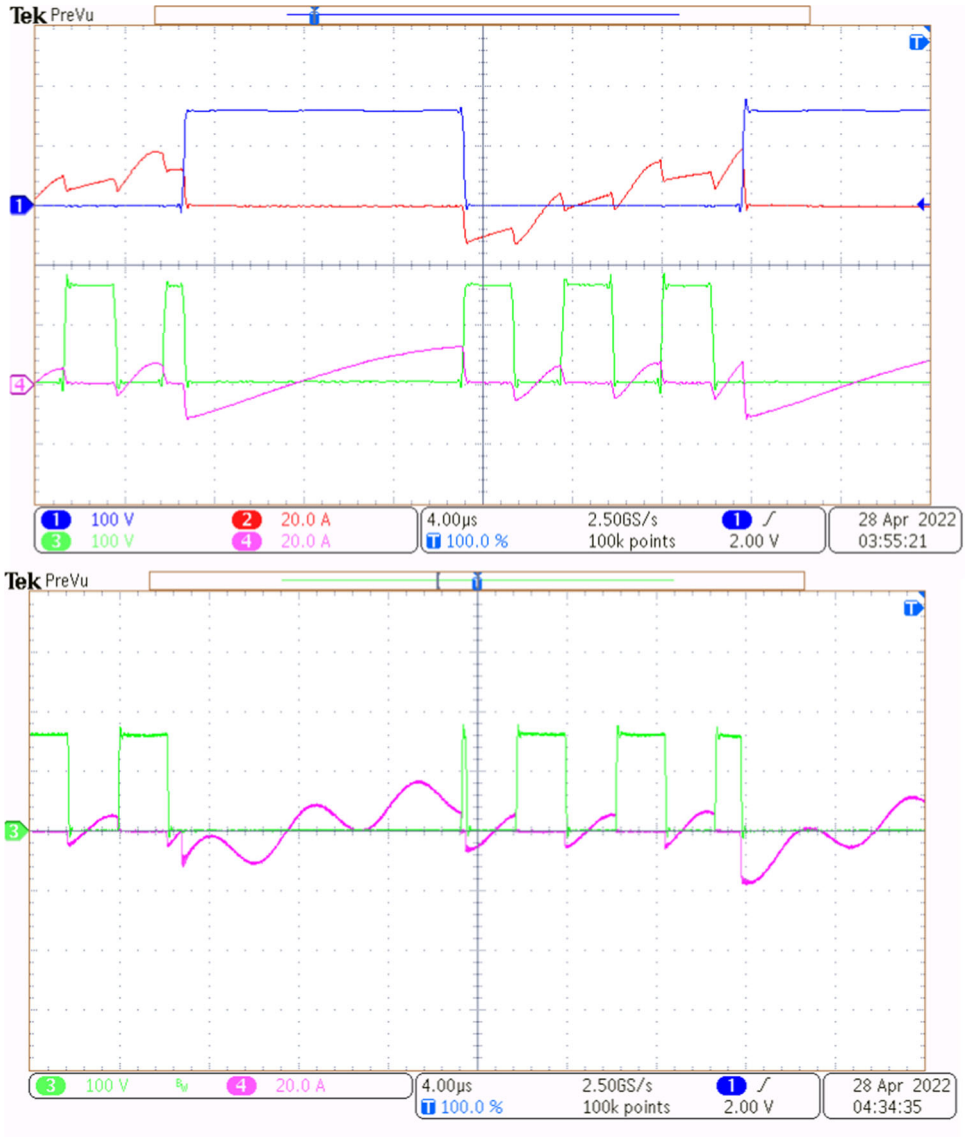

Fig. 8 Experimentation waveforms of switch voltage and currents when P_{st} = 176 W and P_{al} = 76.18 W. From top to bottom: S_1, S_2 and S_3 respectively. Scale: voltage (100 V/div) and current (20 A/div)

It can be observed from above equations that power in aluminum load, P_{al} depends on D_{al}, τ and $T_{st,on}$. By varying the operating frequency f_{al}, the impedance of the circuit and hence the current flowing through aluminum load can be altered. Frequency based control is applied for both the loads. For aluminum load, duty cycle control is also applied. The power in the aluminum load is depending on the D_{st}. To increase maximum power for aluminum load, D_{st} can be increased above 50%. This will reduce the maximum power for steel load which can be compensated by reducing its operating frequency. Analysis of the inverter operation is done with D_{st} = 50% and D_{st} = 65% and is verified through simulation and experimentation.

5 Experimentation results and analysis

The experimental parameters for the inverter are mentioned in Table 1. Two DC power supplies are connected in series to obtain 165 V. Resonant capacitors are obtained by series–parallel combination of MKV-B25834 and MKP-B32672L type capacitors. The complete experimentation setup is shown in Fig. 6. The control for the inverter is realised using an FPGA controller board. The values of D_{st} should be selected as per the maximum powering requirements of both the loads. The inverter prototype has been tested for D_{st} values of 65% and 50%.

The full load output power experimentation results are shown in Fig. 7. For D_{st} = D_{al} = 50% (5050), the results

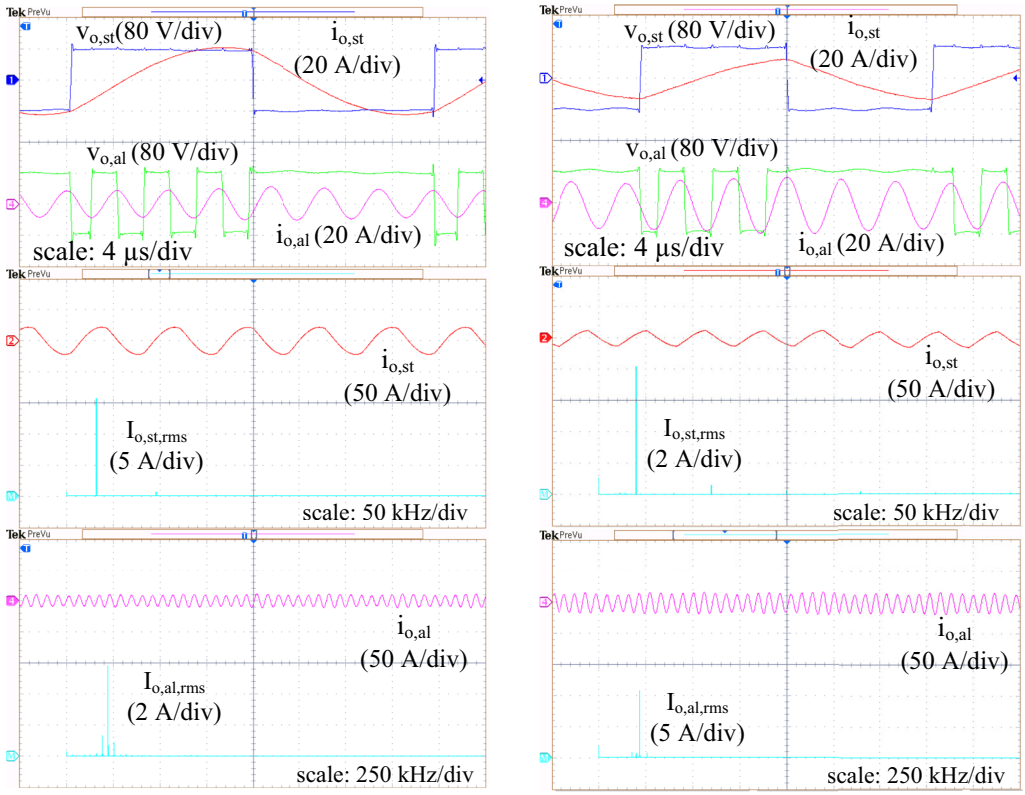

(a) f_{st}=32 kHz and f_{al}=220 kHz

(b) f_{st}=40 kHz and f_{al}=216 kHz

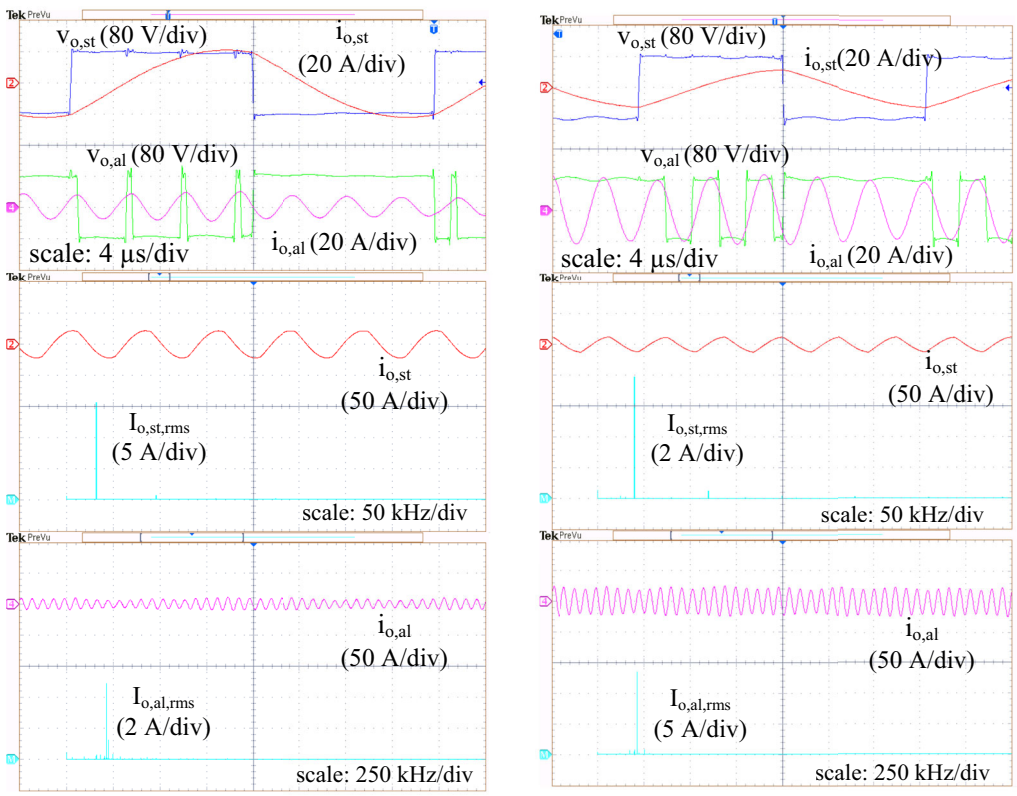

(c) f_{st}=32 kHz and D_{al}=85%

(d) f_{st}=40 kHz and D_{al}=50%

Fig. 9 Variable power operation of 3 S-DFRI with frequency and duty cycle control for D_{st}=50%. From top to bottom: output voltage-current waveforms and load current FFTs for steel and aluminum loads. **a** and **b** D_{al} = 50%. **c** and **d** f_{al}=215 kHz

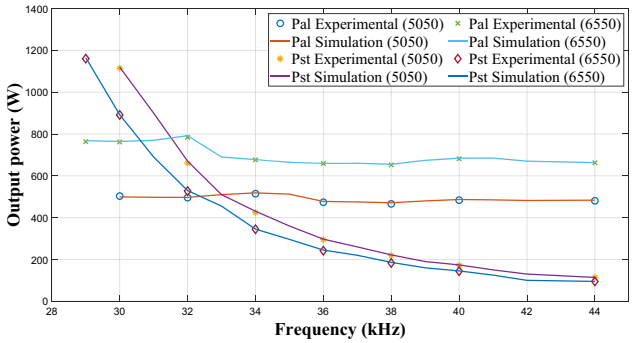

(a) Load power vs f_{st} ($D_{al} = 50\%$ and f_{al}=215 kHz)

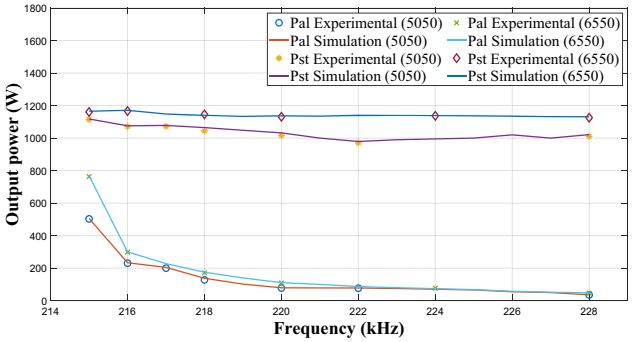

(b) Load power vs f_{al} ($D_{al} = 50\%$)

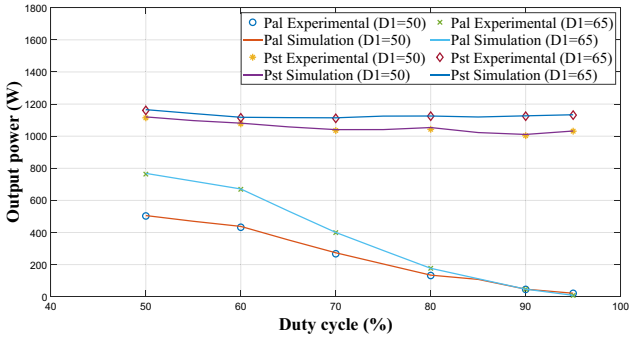

(c) Load power vs D_{al} (f_{al}=215 kHz)

Fig. 10 Output power variation over frequency and duty cycle control

are shown in Fig. 7a. f_{st} and f_{al} are 30 kHz and 215 kHz, respectively. The rms currents flowing through steel and aluminum loads are 19.95 A and 15.86 A, respectively. Steel load is powered at 1114.41 W and aluminum load is powered at 503.08 W. The total power delivered is 1617.49 W. Figure 7b shows the experimental results when D_{st} = 65% and D_{st} = 50% (6550). f_{st} and f_{al} are maintained at 29 kHz and 215 kHz, respectively. The rms currents of 20.36 A and 19.54 A flows through steel and aluminum loads powering them at 1160.68 W and 763.62 W, respectively. Total output load power for the inverter is 1924.3 W. The soft switching operation of three switches for frequency based control (f_{st} = 40 kHz, f_{al} = 224 kHz, $D_{\text{st}} = D_{\text{al}}$ = 50%) when P_{st} = 176 W and P_{al} = 76.18 W is shown in Fig. 8.

The output power variation results are shown in Fig. 9. Figure 9a, b depicts the results for frequency based control for both the loads. Figure 9a shows the experimental results when steel and aluminum loads are powered at 677.1 W and 74.71 W carrying 15.6 A and 6.1 A, respectively. Figure 9b shows the experimental results when steel and aluminum loads are powered at 190 W and 247.3 W carrying 8.24 A and 11.12 A, respectively. Figure 9c, d depicts the results for frequency based control for steel and duty cycle based control for aluminum load. Figure 9c shows the results when steel and aluminum loads currents are 15.5 A and 5.7 A with load powers of 673.57 W and 65.67 W, respectively. Figure 9d shows the results when steel and aluminum load currents are 7.9 A and 15.86 A powering them at 176 W and 503.08 W, respectively.

The graphs of output power variation with frequencies and duty cycles are plotted in Fig. 10. Simulation and experimental results for variable power operation under $D_{\text{st}} = 50\%$ and $D_{\text{st}} = 65\%$ are plotted. And it is observed that simulation and experimental results are in good accord with each other. Figure 10a shows steel load power variation over frequency while aluminum load control parameters are maintained constant. The steel load power is controlled from 1114.41 to 113.62 W and 1160.68 to 94.68 W for $D_{\text{st}} = 50\%$ and $D_{\text{st}} = 65\%$ respectively. D_{al} is also maintained constant at 50% throughout the operation. Figure 10b shows aluminum load power variation over frequency while steel load control parameters are maintained constant. The aluminum load power is controlled from 503.08 W to 35.28 W and 763.62 W to 46.87 W for $D_{\text{st}} = 50\%$ and $D_{\text{st}} = 65\%$, respectively. D_{al} is maintained at 50% constant through the operation. Figure 10c shows the aluminum load power variation with duty cycle while steel load control parameters are maintained constant. With the duty cycle control, aluminum load power

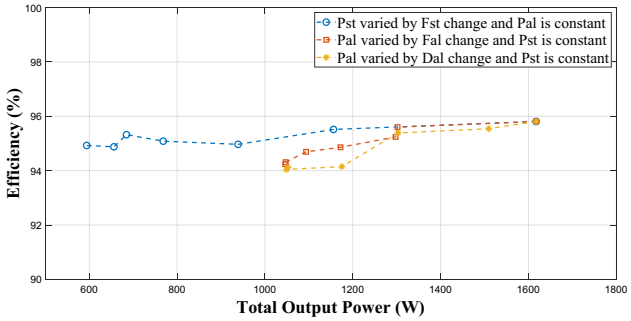

(a) $D_{st} = D_{al} = 50\%$

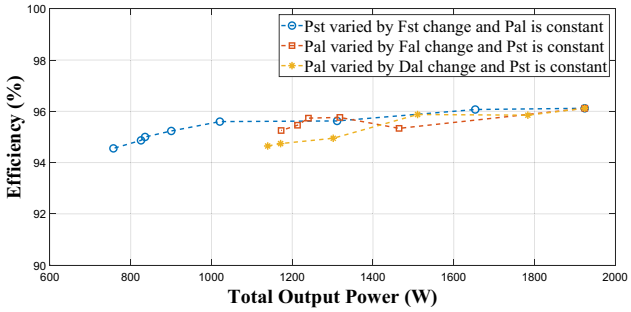

(b) $D_{st} = 65\%$

Fig. 11 Efficiency over total output power variation

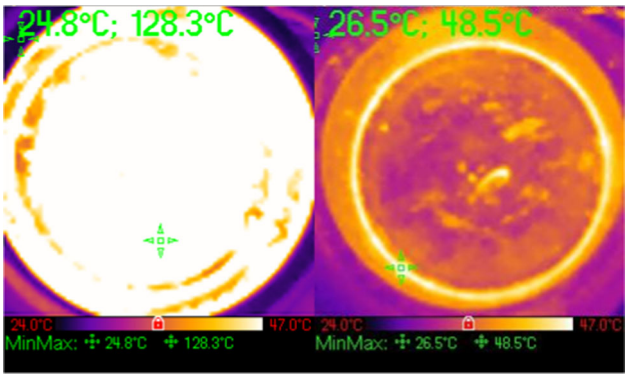

Fig. 12 Thermal images for steel and aluminum vessels at full load condition

is varied from 503.08 to 21.26 W and 763.62 to 8 W for $D_{\text{st}} = 50\%$ and $D_{\text{st}} = 65\%$, respectively. Steel and aluminum load frequencies are maintained constant during the entire operation. The efficiency of the inverter over the total output power variation is plotted in Fig. 11. It can be observed that the inverter operates with more than 94% efficiency for the entire power variation. The peak efficiency offered by the inverter is 96.11%. Thermal images for both the vessels operated at full load for a minute is shown in Fig. 12. The proposed inverter topology is compared with the other existing inverter topologies which are suitable for two different material IH loads and is presented in Table 2. It is observed that the proposed inverter topology offers the advantages of soft-switching operation, high efficiency, independent as well as simultaneous control and low component count without any electro-mechanical switches.

6 Extension of the inverter

The proposed inverter can be extended for multiple different material IH loads. Figure 13 shows the extension of the proposed 3 S-DFRI for four loads. All these four loads can be powered at four different frequencies. Hence, different frequency requirement of the loads can be met and also load powers can be independently controlled. This topology can be extended for multiple IH loads by addition of three switches per two loads. The extension gives provision of four independent frequency component generation as output (Fig. 13).

Table 2 Comparison of IH solutions for different material vessels for two loads

References	Operating frequency (kHz)	Soft switching	Peak efficiency (%)	Independent control	Simultaneous control	No. of switches & diodes	Electromechanical switches	No. of L & C
[20]	20, 50	No	–	Yes	No	2	1	2 coils, 1 C
[21]	23–75	No	96	Yes	No	2	1	1 C
[22]	30,150	Yes	92	Yes	Yes	4	0	1 C
[23]	25–125	Yes	96.5	Yes	No	4	2	1 C
[24]	20,100,400	No	≥92	Yes	Yes	8	0	2 C
[25]	30/78	Yes	94.32	Yes	No	4	1	1 L & 2 C
Proposed 3S-DFRI	29–44, 215–228	Yes	96.11	Yes	Yes	3	0	2 C

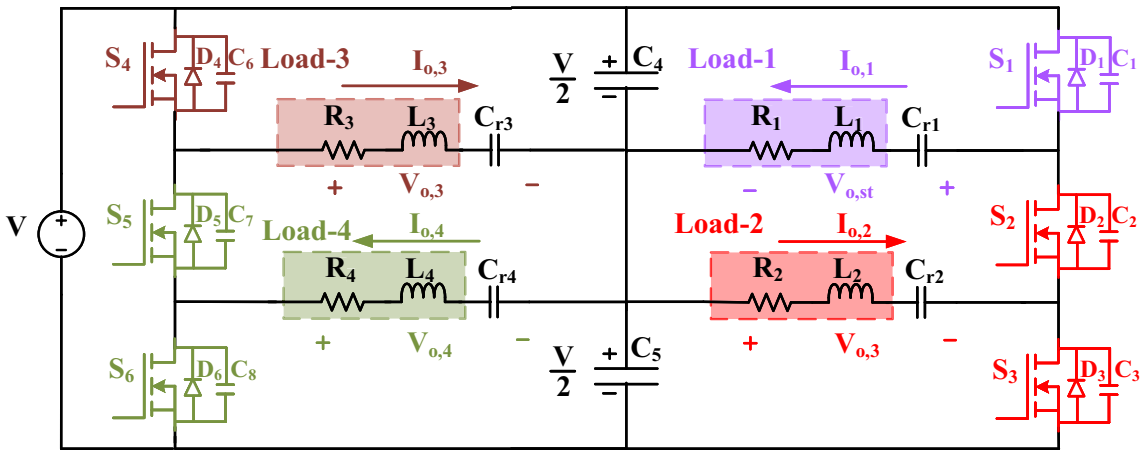

Fig. 13 Extension of the topology with four different IH loads

7 Conclusion

In this research work, an inverter topology with three switch and dual frequency operation suitable for two different material IH loads is proposed. The operation of the proposed inverter and independent power control are verified with rigorous simulation and experimentation. Experimental prototype of the inverter is implemented and tested for nearly 2 kW total output power rating. In this paper, steel and aluminum vessel loads are used for experimentation. It provides peak efficiency of 96.11%. Frequency and duty cycle based controls are used for simultaneous as well as independent control. The proposed solution can be extended for multiple IH loads by three switches per two different IH loads. Low component count, high efficiency, compact solution, simultaneous and independent control are main advantages of the proposed solution for heating vessels of different materials.

Declarations

Conflict of interest The authors have no competing interests to declare that are relevant to the content of this article.

References

1. Su C, Madani H, Palm B (2018) Heating solutions for residential buildings in china: current status and future outlook. Energy Convers Manag 177:493–510. https://doi.org/10.1016/j.enconman.2018.10.005
2. Koller L, Novák B (2017) Improving the energy efficiency of induction cooking 2. Electr Eng 99:171–178. https://doi.org/10.1007/s00202-016-0405-2
3. Koller L, Novák B (2009) Improving the energy efficiency of induction cooking. Electr Eng 91:153–160. https://doi.org/10.1007/s00202-009-0127-9
4. Brown GH, Hoyler CN, Bierwirth RA, et al (1947) Theory and application of radio-frequency heating. Theory and application of radio-frequency heating
5. Ozturk M, Altintas N (2022) Multi-output ac-ac converter for domestic induction heating. Electr Eng. https://doi.org/10.1007/s00202-022-01664-8
6. Salvi B, Porpandiselvi S, Vishwanathan N (2022) A three switch resonant inverter for multiple load induction heating applications. IEEE Trans Power Electron. https://doi.org/10.1109/TPEL.2022.3173931
7. Koertzen H, Ferreria J, Van Wyk J (1992) A comparative study of single switch induction heating converters using novel component effectivity concepts. In: PESC'92 Record. 23rd annual IEEE power electronics specialists conference, pp. 298–305. IEEE. https://doi.org/10.1109/PESC.1992.254659
8. Kamli M, Yamamoto S, Abe M (1996) A 50–150 khz half-bridge inverter for induction heating applications. IEEE Trans Ind Electron 43(1):163–172. https://doi.org/10.1109/41.481422
9. Dede EJ, Gonzalez JV, Linares JA, Jordan J, Ramirez D, Rueda P (1991) 25-kw/50-khz generator for induction heating. IEEE Trans Ind Electron 38(3):203–209. https://doi.org/10.1109/41.87588
10. Salvi B, Vishwanathan N, Porpandiselvi S (2021) A direct ac-ac multiple load inverter for vessels of different materials. In: 2021 National power electronics conference (NPEC), pp. 01–06. IEEE. https://doi.org/10.1109/NPEC52100.2021.9672527
11. Chudjuarjeen S, Sangswang A, Koompai C (2010) An improved *llc* resonant inverter for induction-heating applications with asymmetrical control. IEEE Trans Ind Electron 58(7):2915–2925. https://doi.org/10.1109/TIE.2010.2070779
12. Esteve V, Sanchis-Kilders E, Jordán J, Dede EJ, Cases C, Maset E, Ejea JB, Ferreres A (2011) Improving the efficiency of igbt series-resonant inverters using pulse density modulation. IEEE Trans Ind Electron 58(3):979–987. https://doi.org/10.1109/TIE.2010.2049706
13. Khatroth S, Shunmugam P (2021) Single-stage pulse frequency controlled ac-ac resonant converter for different material vessel induction cooking applications. Int J Circuit Theory Appl 49(9):2865–2884. https://doi.org/10.1002/cta.3042
14. Kumaraswamy A, Bhattacharya A, Sadhu PK (2023) Dual output direct ac-ac series resonant converter for all metal induction heating system with a hybrid control technique. Electr Eng. https://doi.org/10.1007/s00202-023-01743-4
15. Law K, Cheng KE (2008) Examination of the frequency modulation and lifting techniques for the generalized power factor correction switched-capacitor resonant converter. Int J Circuit Theory Appl 36(7):839–855. https://doi.org/10.1002/cta.462
16. Fujita A, Sadakata H, Hirota I, Omori H, Nakaoka M (2009) Latest developments of high-frequency series load resonant inverter

type built-in cooktops for induction heated all metallic appliances. In: 2009 IEEE 6th international power electronics and motion control conference, pp. 2537–2544. IEEE. https://doi.org/10.1109/IPEMC.2009.5157832
17. Han W, Chau K, Lam W (2019) All-utensil domestic induction heating system. Energy Convers Manag 195:1035–1043. https://doi.org/10.1016/j.enconman.2019.05.093
18. Rodriguez JI, Leeb SB (2009) Nonresonant and resonant frequency-selectable induction-heating targets. IEEE Trans Ind Electron 57(9):3095–3108. https://doi.org/10.1109/TIE.2009.2037676
19. Meng L, Cheng KE, Chan KW, Lu Y (2012) Variable turn pitch coils design for heating performance enhancement of commercial induction cooker. IET Power Electron 5(1):134–141. https://doi.org/10.1049/iet-pel.2010.0388
20. Tanaka T (1989) A new induction cooking range for heating any kind of metal vessels. IEEE Trans Consum Electron 35(3):635–641. https://doi.org/10.1109/30.44329
21. Millan I, Burdío J, Acero J, Lucía O, Llorente S (2011) Series resonant inverter with selective harmonic operation applied to all-metal domestic induction heating. IET Power Electron 4(5):587–592. https://doi.org/10.1049/iet-pel.2010.0107
22. Papani SK, Neti V, Murthy BK (2015) Dual frequency inverter configuration for multiple-load induction cooking application. IET Power Electron 8(4):591–601. https://doi.org/10.1049/iet-pel.2014.0114
23. Park H-P, Jung J-H (2018) Load-adaptive modulation of a series-resonant inverter for all-metal induction heating applications. IEEE Trans Ind Electron 65(9):6983–6993. https://doi.org/10.1109/TIE.2018.2793270
24. Khatroth S, Shunmugam P (2020) Cascaded full-bridge resonant inverter configuration for different material vessel induction cooking. IET Power Electron 13(19):4428–4438. https://doi.org/10.1049/iet-pel.2020.0728
25. Han W, Chau KT, Liu W, Tian X, Wang H (2021) A dual-resonant topology-reconfigurable inverter for all-metal induction heating. IEEE J Emerg Sel Top Power Electron. https://doi.org/10.1109/JESTPE.2021.3071700